



Article

An Improved Method for the Evaluation and Local Multi-Scale Optimization of the Automatic Extraction of Slope Units in Complex Terrains

Zhongkang Yang^{1,2}, Jinbing Wei^{1,2,*}, Jianhui Deng^{1,2}  and Siyuan Zhao^{1,2}

¹ State Key Laboratory of Hydraulics and Mountain River Engineering, Chengdu 610065, China; yangzhk@stu.scu.edu.cn (Z.Y.); jhdeng@scu.edu.cn (J.D.); zhaosiyuan@scu.edu.cn (S.Z.)

² College of Water Resource and Hydropower, Sichuan University, Chengdu 610065, China

* Correspondence: jbwei@scu.edu.cn

Abstract: Slope units (SUs) are sub-watersheds bounded by ridge and valley lines. A slope unit reflects the physical relationship between landslides and geomorphological features and is especially useful for landslide sensitivity modeling. There have been significant algorithmic advances in the automatic delineation of SUs. But the intrinsic difficulties of determining input parameters and correcting for unreasonable SUs have hindered their wide application. An improved method of the evaluation and local multi-scale optimization for the automatic extraction of SUs is proposed. The SUs' groups more consistent with the topographic features were achieved through a stepwise approach from a global optimum to a local refining. First, the preliminary subdivisions of multiple SUs were obtained based on the r.slopeunit software. The optimal subdivision scale was obtained by a collaborative evaluation approach capable of simultaneously measuring objective minimum discrepancies and seeking a global optimum. Second, under the selected optimal scale, unreasonable SUs such as over-subdivided slope units (OSSUs) and under-subdivided slope units (USSUs) were further distinguished. The local average similarity (*LS*) metric for each SU was designed based on calculating the SU's area, common boundary and neighborhood variability. The inflection points of the cumulative frequency curve of *LS* were calculated as the distinguishing intervals for those unrealistic SUs by maximum interclass variance threshold. Third, a new effective optimization mechanism containing the re-subdivision of USSUs and merging of OSSUs was put into effect. We thus obtained SUs composed of terrain subdivisions with multiple scales, which is currently one of the few available methods for non-single scales. The statistical distributions of density, size and shapes demonstrate the excellent performance of the refined SUs in capturing the variability of complex terrains. Benefiting from the sufficient integrating approach of diverse features for each object, it is a significant advantage that the processing object can be transferred from general entirety to each precise individual.

Keywords: slope units; digital elevation model; optimum subdivision parameters; refinement; terrain adaptability



Citation: Yang, Z.; Wei, J.; Deng, J.; Zhao, S. An Improved Method for the Evaluation and Local Multi-Scale Optimization of the Automatic Extraction of Slope Units in Complex Terrains. *Remote Sens.* **2022**, *14*, 3444. <https://doi.org/10.3390/rs14143444>

Academic Editor: Xinghua Li

Received: 10 June 2022

Accepted: 15 July 2022

Published: 18 July 2022

Publisher's Note: MDPI stays neutral with regard to jurisdictional claims in published maps and institutional affiliations.



Copyright: © 2022 by the authors. Licensee MDPI, Basel, Switzerland. This article is an open access article distributed under the terms and conditions of the Creative Commons Attribution (CC BY) license (<https://creativecommons.org/licenses/by/4.0/>).

1. Introduction

Regional landslide risk assessment has been shown to be an effective tool for mitigating casualties and property damage caused by landslide hazards [1]. To obtain reliable assessments of landslide risks, it is crucial to first select an appropriate mapping unit for extracting and distributing geoenvironmental data [2]. Common mapping units mainly include grid units, slope units (SUs), terrain units and unique condition units [3]. SUs are associated with the geomorphological process shaping the natural morphology, and thus reflect the physical relationships between landslides and the environmental information [4]. Therefore, SUs are especially suitable for landslide sensitivity modeling [5,6]. The acquisition and application of SUs have received increased attention [7].

Following traditional hydrological principles, SUs are defined as the intersecting zones of a drainage ridge and a catchment's valley line [8]. The ridge line is the boundary of the basin, and the space in the middle of two ridgelines is the catchment area. The valley line is extracted to slice the basin, and two SUs can be obtained [9]. Accordingly, the forward and reverse digital elevation model (DEM) hydrological analysis method was developed to extract SUs automatically and is currently one of the most used and reliable methods [10]. However, geomorphologically, those SUs correspond not only to the single slopes, but also to multiple slopes or even an entire watershed [11]. Some new definitions and constraints for SUs have been added to basic hydrological process analyses. The SUs should be an area with distinctly different topographic features from the adjacent areas [12]. In addition to ridge and valley lines, topographic discontinuities in aspect, slope and curvature should also be used and serve as dividing lines [3,13]. Consequently, aspect-based methods [14,15] curvature-based methods [16,17], and regional growth-based methods [18,19] have been successively developed to perform automatic extraction of SUs. For aspect-based methods of the r.slopeunits software, the SUs are still defined as the intersecting zones by hydrological drainage and dividing lines, and the slope aspect is taken as a new constraint for measuring external heterogeneity and internal homogeneity [14,15]. Furthermore, the SUs are defined as continuous and enclosed regions of uniform slope gradient and direction by curvature-based methods [16,17]. These emerging methods are significant improvements over the previous hydrological methods in terms of automation and refinement of SUs extraction.

However, with the increase in complexity and multi-class parameters setting, determining input parameters is becoming one of the main obstacles for the automated methods [18]. The input parameters have to be determined by the user based on expertise, with a trial-and-error approach [20,21]. Compromising between coarser and finer segmentation is the main strategy for obtaining the final scale parameters [22]. There is a lack of quantitative metrics to guide the selection of appropriate segmentation parameters [23]. Huang et al. [18] proposed an improved supervised trial-and-error method. The extracted image objects are realistic when the errors between the recorded landslides and the SUs area and shape index are within a certain threshold. In addition, Alvioli et al. [14,15] proposed the global score (*GS*) combining global variance and Global Moran's *I* (*MI*) as a practicable unsupervised evaluation method. The optimal scale can be identified by taking into account global interior and external heterogeneity [24]. The evaluation approaches contribute to removing subjectivity from the algorithm and produce more objective results. However, there is a lack of explicit scientific justification for the matching between the global optimal scale and actual land surface discontinuities. This is a common defect for unsupervised evaluation methods [25]. Moreover, a normalization step is required for each global *MI* and variance before obtaining the *GS* value. Thus, under the undefined candidate SUs' groups, the *GS* value would be uncertain with the changing extrema in *MI* or variance [26]. The inconsistent optimal scale would occur correspondingly. Unstable optimal scale results can be eliminated only once meaningful and realistic SUs sets are selected. Therefore, the supervised and unsupervised evaluation approaches can be integrally exploited for determining the optimal scale parameter [23].

Despite the rigorous and logical procedure, many unrealistic SUs are still frequently observed at the selected optimal scale when using automatic delineation [15]. This is the consequence of using constant criteria and a common problem of existing automated methods [15,18]. There are significant differences in geographical and geomorphological conditions in various high mountain and hilly regions, leading to corresponding differences in scale and shape features of SUs. A stationary scale can only realize the proper terrain subdivision of the landscape with certain area and shape characteristics. Others that produce unreasonable SUs that are not consistent with the terrain may be sacrificed. Those undesirable objects are defined as over-segmented and under-segmented problems in the field of land cover classification, image segmentation, target detection and other related image analyses [27,28]. It is a frontier hot topic and quite a few studies have been

devoted to the continuous optimization of subsequent unrealistic objects after one “optimal” segmentation [29,30]. The identification and combination of multiple scales have been shown to help resolve undesirable objects [31]. The concepts of over-subdivision and under-subdivision are equally applicable to classifying undesirable SUs. Unfortunately, the problem of continuous optimization for the subsequently unreasonable SUs has always been ignored by researchers, and the corresponding solutions are not tried.

To improve the production of objective and reproducible SUs and make up for the lack of subsequent amending for unrealistic SUs, an improved quality evaluation and local multi-scale optimization method for automatically extracting SUs in complex terrains is proposed. The optimal scale criterion for delineating SUs, and effective integration of diverse spatial features into refinements of unrealistic SUs are demonstrated in this paper. It is the first application for improvement of individual SUs’ objects from automatic subdivision procedures and from which SUs consisted of terrain subdivisions with multiple scales are obtained.

2. Study Area and Data Preparation

2.1. Study Area

The Yuqu River Basin is at the southeastern margin of the Tibetan Plateau and is a tributary on the left bank of the Salween River (latitude/longitude: $28^{\circ}24'49''\sim 30^{\circ}11'41''$, $97^{\circ}22'24''\sim 98^{\circ}41'41''$) (Figure 1a). The region forms a typical high mountain and canyon landform. The total study area is 9190 km^2 , with a river drop of 2122 m (Figure 1b). It can be divided into a high hilly zone, a middle high-mountain zone, a gorge transition zone and an alpine gorge according to altitude and topography [32,33] (Figure 1c). The high hilly zone (I) alternates the distribution of an open intermountain basin and rounded mountains, of which the valley bottom width is 800~5000 m. The middle high-mountain zone (II) is a widely developed glacier erosion and accumulation landform, located in the northeast highlands at 4300~5800 m elevation. The gorge transition zone (III) is an erosional mountain with a “U” type river valley, with an average gradient of 0.69%. River floodplains and multi-level terraces are generally developed and have a valley width of 50~800 m. The alpine gorge zone (IV) is located downstream of the river and has an elevation of 1800~3200 m. The width of the deep “V” valley is only 40~80 m and the flow is turbulent, with an average gradient of 1.12%.

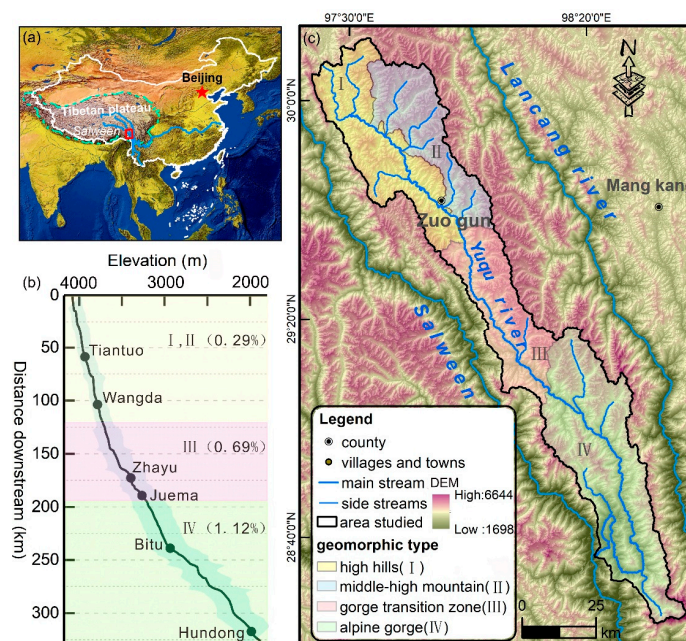


Figure 1. (a) Location of Yuqu River Basin in Tibetan Plateau. (b) The Yuqu River profile line. (c) Shade relief of DEM and the I, II, III and IV geomorphic zones.

2.2. Data Preparation

The Advanced Land Observing Satellite-1 from the Japan Aerospace Exploration Agency (JAXA) provides ALOS-12m DEM data with a spatial resolution of 12.5 m (Figure 2a). Remote sensing images were obtained from the Gaofen-2 satellite data acquired on 20 January 2020, and a true color image covering the Yuqu River Basin at 1-m spatial resolution was obtained (Figure 2b). The hillshade of the DEM and images unified into the projection coordinate system WGS 1984/UTM Zone 47N, were imported in ArcScene 10.6.1 to obtain the three-dimensional terrain representation. Actual comparison photos of typical locations are obtained by using an unmanned air vehicle (Phantom 4pro V2.0 by DJI Innovation Technology Co., Ltd., Shenzhen, China, flight altitude 500 m) in field investigations (Figure 2c).

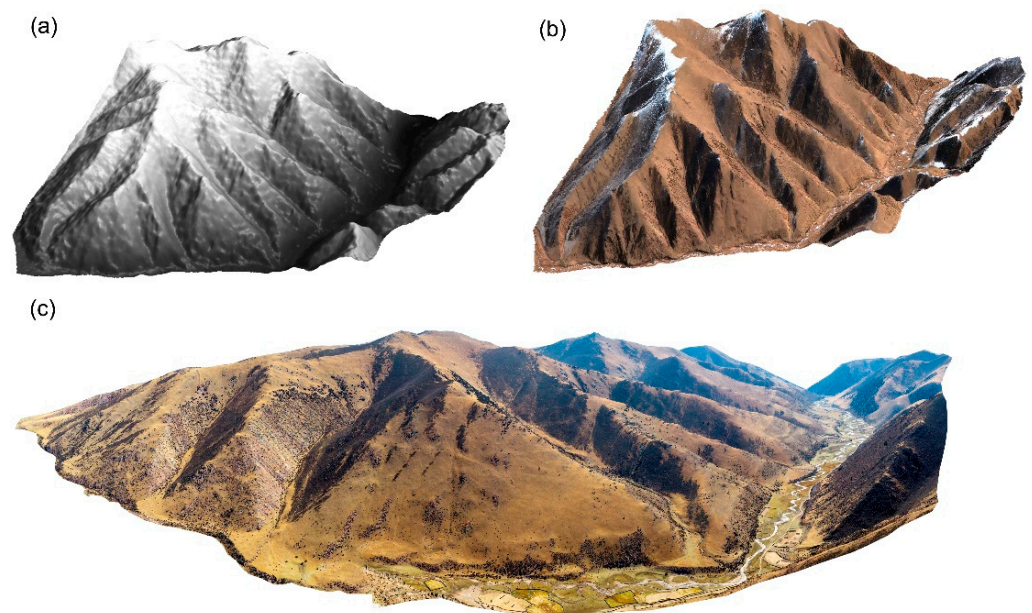


Figure 2. Examples of data used in the study, (a) hillshade from DEM, (b) true color Gaofen-2 satellite image, and (c) the photo in the same region.

2.3. Reference SUs

The reference SUs play a crucial role in the evaluation of optimal scale for the automatically extracted SUs. To obtain normative reference samples, the following procedures are performed: (1) The forward and reverse DEM hydrological analysis method is selected to obtain the sub-basins divided by drainage lines and dividing lines. The method conforms to researchers' original definition of SUs, and detailed and common rules can be referenced to obtain undisputed results [8–10]. Based on the ArcGIS Hydrological analysis tool, the extraction of ridgelines mainly includes depression filling, flow direction extracting, flow accumulation setting, river network extracting, obtaining catchment area [10]. The extraction of valley lines is obtained through reversing DEM, performing the same steps as for ridgelines [10,34]. According to previous studies on the adjacent regions [35,36], the appropriate catchment area thresholds are at the axis between river network density and catchment area [18,36]. As is shown in Figure 3b, the catchment area threshold of positive topography is 3000 pixels, and the negative topography is 3500 pixels. The filling thresholds are set as the recommended defaults (Table 1). (2) In order to pick out the single slopes and reject multiple slopes or even an entire watershed from the sub-basins, the circular variance of aspect is taken as measure of homogeneity for each subregion. Referring to experience about the subdivision of SUs from Alvioli et al. [14,15] and Jacobs et al. [5], only the sub-basins of aspect circular variance (c) between 0.20–0.30 are selected as candidate reference SUs. (3) To improve the validity and typicality of those samples, regular hexagonal grid

zones are created to implement an equally spaced sampling strategy. The abnormal parallel pseudo valleys (Figure 3a(B)) are abandoned and manually labelled as non-sampling zones, which is the limitation inherent in the hydrological analysis method. Taking each hexagon of sampling zones as the center (Figure 3a(A)), the candidate SUs with the largest size in the statistical area are selected as reference SUs. As is shown in Figure 3c,d, the sub-basins C with uniform aspect and proper size are more suitable as reference objects in that hexagon grid zone. (4) Based on the commonly used criteria for estimating the sampling quantity (the confidence level, 95%; the confidence interval, 3%) [37] and 8875 sub-basins as references for estimating the total number of SUs, an appropriate sampling size of reference SUs should be 952. Accordingly, the research area was divided into 1011 square hexagonal grids, 59 of which were marked as non-sampling zones, leaving 952 sampling zones to generate reference SUs (Figure 3a).

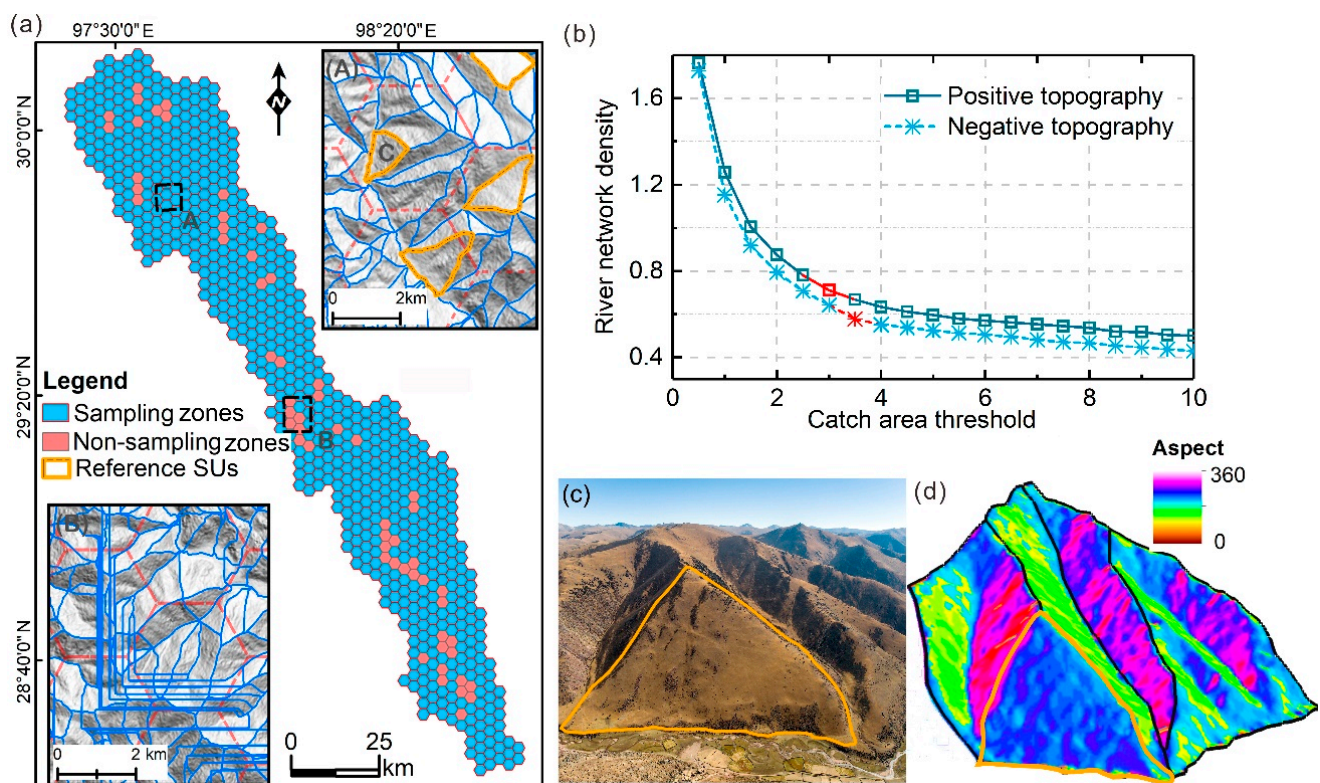


Figure 3. The spatial distribution and examples of reference SUs. (a) is the spatial distribution of sampling sites of reference SUs. (b) is the relationship between river network density and catchment area threshold. (c,d) is the scene photo and slope aspect of reference SU C, respectively.

Table 1. Parameters Guide for obtaining reference SUs.

Parameters	Criterion	Reference
Filling threshold	(Positive topography) 40 m; (Negative topography) 60 m	[35,36,38]
Catchment area	(Positive topography) 3000 pixels; (Negative topography) 3500 pixels	[35,36,38]
Aspect circular variance	$0.20 \leq c \leq 0.30$	[14,15,39]
Area	The maximum area of candidate reference SU in each sampling zone	[14]

3. Methodology

Given the challenges in the determination of the optimal scale and refining of unrealistic SUs, this study proposes an iterative process to achieve SUs more consistent with the terrain (Figure 4). (1) Multiple sets of the preliminary SUs are created by the r.slopeunits v1.0 (created by Ivan Marchesini and Massimiliano Alvioli, Perugia, Italy)

with multi-parameter combinations. (2) The candidate SUs of good consistency with the referenced SUs by the measurement of object consistency error (OCE) are selected. Then, the Global Moran's I indicating external heterogeneity and global variance to denote the internal homogeneity are combined and used for the final determination of an optimal subdivision scale. (3) The local average similarity (LS) with consideration of the spatial area, common boundary, and neighborhood mutation properties of each SU is created for the identification of OSSUs and USSUs. (4) Based on multiple local heterogeneities and potential homogeneity changes, the merging criterion and effective verification procedure are designed for optimizing the improper SUs.

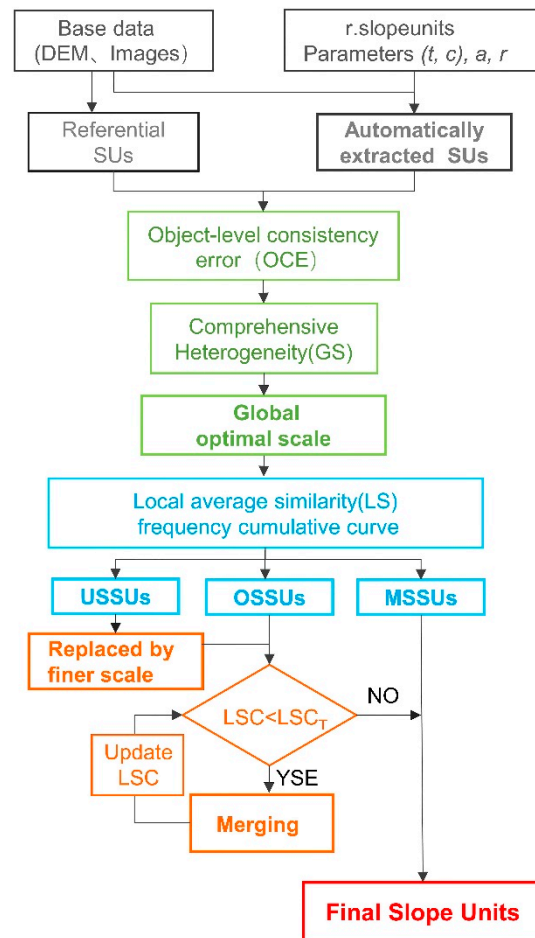


Figure 4. Flow diagram of the proposed assessment and local multi-scale optimization method.

3.1. Initial Subdivision of SUs

Due to its extensive use and demonstrated skill in capturing the aspect variability of the landscape [5,15,39], the r.slopeunits software v1.0 (Ivan Marchesini and Massimiliano Alvioli, Perugian, Italy) was adopted to obtain the multiple groups of the preliminary subdivision of SUs. Given a DEM and some input parameters, the algorithm first partitions the digital topography into several larger half basins (HBs); then, the sub-basins are continuously divided under the reduced factor (r) of the initial flow accumulation area threshold (t) in each iteration [39]. When the child of an HB matches the user-defined parameters of minimum area (a) and circular variance (c), it is selected as a candidate SU and the iterative procedure ends. The software of r.slopeunits v1.0 was obtained from the portal of the Geomorphology Research Group (<http://geomorphology.irpi.cnr.it/tools/slope-units> (accessed on 10 June 2022)). Users need to define the following parameters: the initial flow accumulation area threshold (t), minimum surface area (a), minimum circular variance (c), reduction factor (r), threshold value for the cleaning procedures (*Cleansize*).

3.2. Determination of the Optimal Subdivision Scale

3.2.1. Object-Level Consistency Error (OCE)

The ability to explicitly calculate the error between the automatically extracted SUs and the reference SUs from the ground truth is of prior importance in our assessment framework. It is the first step for eliminating the unreasonable SUs result. The common error measures are constructed by regarding the assessment as a process of intersection (correct) or difference (wrong) pixel labeling [40,41]. Consequently, it cannot accurately distinguish the error originated from under-subdivision or over-subdivision. When the combination of multiple extracted SUs is exactly the same as reference SUs, the error measure would consider the two to be consistent. Therefore, the object level consistency error (OCE) was introduced to evaluate the performance of extracted SUs objectively [25]. The error measures are based on object-by-object comparisons of extracted SUs and reference SUs. Compared to existing error measures, it can take into account the size, shape, and position of each recorded SUs at the object level. Moreover, it is sensitive to both under-subdivision and over-subdivision, which contributes to make reasonable inferences from stepwise errors evolution analyses. The OCE is calculated as:

$$OCE(I_g, I_s) = \min(E_{g,s}, E_{s,g}) \quad (1)$$

where $E_{g,s}$ represents the part error of automatically extracted SUs to reference SUs, and $E_{s,g}$ represents the part error of reference SUs compared to automatically extracted SUs. The part error $E_{g,s}$ is measured as:

$$\begin{aligned} E_{g,s}(I_g, I_s) &= \sum_{j=1}^M \left[1 - \sum_{i=1}^N \frac{|A_j \cap B_i|}{|A_j \cup B_i|} \times W_{ji} \right] w_j, \\ W_{ji} &= \frac{\bar{\delta}(|A_j \cap B_i|)|B_i|}{\sum_{k=1}^N \bar{\delta}(|A_j \cap B_k|)|B_k|}, \\ W_j &= \frac{|A_j|}{\sum_{l=1}^M |A_l|} \end{aligned} \quad (2)$$

where $I_g = \{A_1, A_2, \dots, A_M\}$ is the reference SUs, and A_j is the j th SU in I_g ; $I_s = \{B_1, B_2, \dots, B_N\}$ is the automatically extracted SUs, and B_i is the i th SU in I_s ; $|A_j|$ represents the number of grid cells in A_j ; $|A_j \cap B_i|$ and $|A_j \cup B_i|$ denotes the intersection and combination of A_j and B_i , respectively; W_{ji} weights each B_i that intersects with A_j according to the size of B_i relative to all grid cells in I_s that intersect with A_j ; W_j weights the importance of A_j relative to I_g ; $\bar{\delta}(x)$ is the delta function. In addition, $E_{g,s}$ is calculated by replacing A_j and B_i in Equation (2).

OCE is normalized between [0, 1], where 0 means completely consistent without error, 1 means completely mismatched. It is generally considered that $OCE < 0.35$ has good consistent matching [25,27]. The standardized acquisition of ground truth (reference) objects is fundamental to the proper functioning of OCE. The lack of explicit correspondence between historical landslides and extracted SUs is not recommended as reference objects. Experts should widely accept high quality reference SUs following detailed processing guidelines to eliminate subjectivity and enhance reproducibility.

3.2.2. Global Optimal Heterogeneity

A moderate scale of subdivision of the terrain is also required to pursue a global optimal optimum. All the SUs should maximize the internal and external heterogeneity. The SUs closest to this assumption should be selected as the global optimal scale. The Global Moran's Index (MI) and global variance (V) are adopted to make a straight-

forward evaluation of external heterogeneity and internal homogeneity, respectively [42]. The two quantities are calculated by Equations (3) and (4):

$$MI = \frac{m \sum_{i=1}^m \sum_{h=1}^m w_{ih} (y_i - \bar{y})(y_h - \bar{y})}{\sum_{i=1}^m (y_i - \bar{y}) (\sum_{i \neq h} \sum w_{ih})} \quad (3)$$

$$V = \frac{\sum_{i=1}^m s_i c_i}{\sum_{i=1}^m s_i} \quad (4)$$

where m is the total number of SUs; w_{ih} is an indicator for spatial proximity, whose value equals 1 when SU_h and SU_i share a common border, 0 otherwise; y_i is the average aspect of SU_i , \bar{y} is the average aspect of the whole terrain aspect; s_i and c_i are the area and circular variance of SU_i . Note that the angle is needed to convert to radians. The average values and the difference should be intended vectorially following the equation in Alvioli et al. [15].

The global heterogeneity score (GS) is calculated by Equation (5):

$$GS = \frac{V_{\max} - V}{V_{\max} - V_{\min}} + \frac{MI_{\max} - MI}{MI_{\max} - MI_{\min}} \quad (5)$$

The group of highest GS is considered to achieve the maximum balance of the internal homogeneity and external heterogeneity and identified as the best subdivision. However, as the candidate SU scale sets gradually increase, the maximum or minimum of MI and V may change accordingly and so does the highest GS value. To compensate for the uncertainty in confirming the optimal scale in existing methods, a combinative use of the OCE strategy is implemented. The measures of OCE are first performed to filter out unrealistic terrain subdivisions, and then qualified SU groups are left to participate in the calculation of GS values.

3.3. Identification of USSUs and OSSUs

Accurately distinguishing these unreasonable SUs is critical for subsequent providing refining objects. In this section, a new metric is designed to automatically detect those unrealistic SUs and categorize them as USSUs and OSSUs. Their specificities are summarized from field investigation and three-dimensional topographic analysis. From a general impression, the USSUs form a larger area than their adjacencies, and a loose boundary along the landform. They have stronger aspect differences between their adjacencies and low intra-unit similarity. Correspondingly, the OSSUs have smaller and more fragmented sizes than normal units. They are usually mixed with surrounding SUs and share a relatively long common boundary. Thus, the OSSUs have higher intra-unit similarity and few differences in aspect with their adjacencies.

To compare the similarity and difference of each unit in a more reasonable way, we took the indirect value of the neighborhood variability of aspect difference or standard deviation rather than their direct values. The average value of all the adjacent SUs was taken as the reference standard of the normal level. The ratio of the SU value to the average value was the neighborhood variability. When the ratio was far from 1, the magnitude of the difference from the normal value was highlighted.

Firstly, the interior similarity and adjacent differences for each SU were determined by the neighborhood variability of aspect difference (D^a) and the neighborhood variability of aspect standard deviation (D^{sd}), as shown in Equations (6) and (8), respectively.

$$D^a_i = Y_i / (\bar{Y}_i) = Y_i / \left(\frac{\sum_{i \neq m}^m w_{im} Y_m}{\sum_{i \neq m} w_{im}} \right) \quad (6)$$

$$Y_i = \left(\frac{\sum_{i \neq m}^m w_{im} |y_i - y_m|}{\sum_{i \neq m} w_{im}} \right) \quad (7)$$

$$D^{sd}_i = \overline{SD}_i / SD_i = \frac{\sum_{i \neq m}^m w_{im} SD_m}{\sum_{i \neq m} w_{im}} / SD_i \quad (8)$$

where Y_i and \bar{Y}_i is the aspect difference of SU_i and the average value difference with its adjacent SUs, respectively; y_i , w_{im} are defined as in Equation (3); SD_i and \overline{SD}_i is the standard deviation of SU_i and the average value of its adjacent SUs, respectively.

These SUs conflicted with the original terrain discontinuity, and had spatial features that were too large, too small, or oddly shaped. Secondly, to improve the accuracy of the identification, the diversity of the SUs's size and boundary were considered by introducing the area ratio (r^a) and the length ratio (r^l), respectively. The area ratio r^a for each SU was calculated as in Equation (9), where a_i and a_m was the s area of SU_i and its adjacent SUs, respectively. The length ratio r^l was the maximum length of the common boundary to its perimeter, calculated using the Equation (10), indicating the degree of coincidence of the common boundary. Where p_i and l_{in} were the perimeter of SU_i and the length of common boundary of its adjacent SUs, respectively:

$$r^a_i = a_i / \sum_i^m w_{im} a_m \quad (9)$$

$$r^l_i = \frac{\max[l_{i_1}, l_{i_2}, l_{i_3}, \dots, l_{i_n}]}{p_i} \quad (10)$$

Subsequently, the area, boundary and aspect difference were integrated into local heterogeneity he^L , which was calculated with Equation (11). Similarly, the area and aspect uniformity were integrated into local homogeneity ho^L and calculated with Equation (12).

$$he^L_i = \left(r^a_i + \frac{1}{1+r^l_i} \right) D^a_i{}^2 \quad (11)$$

$$ho^L_i = \frac{1}{1+r^a_i} D^{sd}_i{}^2 \quad (12)$$

The design structure of the formulas was ingenious. Taken he^L for example, the form of the square power function could enhance specificity with D^a larger than 1. The part of $\left(r^a_i + \frac{1}{1+r^l_i} \right)$ was a combinatorial representation of the SU's local area feature and boundary morphology, acting as the coefficient of D^a . The single excessive D^a was neutralized with smaller coefficients when the area and common boundary of the SUs were not in accord with USSUs, thereby reducing the probability of being misjudged.

Finally, after performing a normalization procedure for he^L and ho^L , a general algebraic formula was employed to characterize the quantitative comparison of two parts [27].

The metric of local average similarity (LS) for each SU was calculated with Equation (13), where the LS was in the range $[-1, 1]$.

$$LS_i = \frac{ho^L_i - he^L_i}{ho^L_i + he^L_i} \quad (13)$$

It is easily inferred that a higher LS represented the stronger nature of ho^L (local homogeneity) and was preferred to be identified as an OSSU. Conversely, a smaller or even close to -1 LS , represented the SUs with weak ho^L but high he^L (local heterogeneity), which is in accord with an USSU.

The metric of local similarity was able to transform the evaluation object from a general entirety to each precise individual, which was an obvious improvement in evaluation scales. For demonstrating the role of spatial boundary features and neighborhood variability in the identification of OSSUs and USSUs, three local similarities (LS) from different variables were prepared: (1) No A condition, where the factors related to difference D^a or standard deviation D^{sd} were replaced with the actual value; (2) No B condition, where the factor related to spatial size and boundary as r^a and r^l were discarded; (3) A and B condition, where both of the spatial features and neighborhood variability were taken into account.

The histogram frequency diagram of LS was established to demonstrate the distribution of the SUs with different properties at the optimal scale. Through the dual inspection of OCE and GS value, the selected optimal scale can make the majority of SUs consistent with the subdivision of the terrain and they were defined as moderate-subdivided SUs (MSSUs). The remaining small part of specific local heterogeneity or homogeneity was concentrated near the 1 or -1 of LS . The X-axis is the LS value, and 40 intervals of 0.05 were assigned in the range $[-1, 1]$. The discontinuity points of curve shapes on $[-1, 0]$ and $[0, 1]$ were used as threshold intervals to distinguish the USSUs, MSSUs and OSSUs. The discontinuities were calculated by the maximum between-cluster variance (Otsu) method [43].

3.4. The Optimization of USSUs and OSSUs

Setting separately variable (smaller or larger) scales for certain parts during the delineation of SUs remained a conceptual problem with operational difficulty [44]. After being marked as unrealistic SUs, a new effective optimization mechanism containing the re-subdivision of USSUs and merging of OSSUs was put into effect.

Firstly, the regions related to USSUs were substituted by corresponding SUs in multiple finer subdivisions, following which the substitution of the highest GS was considered as the best. Nevertheless, the optimal substitution could not guarantee to be the proper terrain re-subdivision for all coexisting USSUs. Some substitutions might generate new subdivisions. Therefore, the re-subdivision of SUs will be marked as OSSUs for examination in the next optimization stage.

Then, although those aggregated and adjacent SUs could be amended conveniently and effectively through merging, the technical difficulties were merging sequences and preventing excessive merging. Referring to Section 3.3, the sub-region merging metrics of local similarity change (LSC) were defined. The principles of LSC merger guidelines were as follows: on the one hand, local heterogeneity (he^L) had a fundamental effect on determining the merging order. Among two or more neighboring OSSUs, the one of lower local heterogeneity had merging priority. On the other hand, the internal homogeneity changes between the new SUs and the original SUs needed to be estimated. The merging between quite different SUs could generate new SUs with complex internal structures. It is the situation of over-merging and should be avoided. The formula mode is shown in Equation (14), and each OSSU can obtain the value by merging with its adjacent and largest SUs.

$$LSC_A = he^L_{Ae} [y_C SD_C - \frac{1}{2}(y_A SD_A + y_B SD_B)] \quad (14)$$

where SU_C is the new SU generated by the SU_A merges with its adjacent SU_B . y is the average aspect of SU and acts as the weight of the standard deviation, which are combined

to represent the uniformity of SU. A given threshold of LSC_T is used for quantifying those excessive merging situations. The LSC_T is consulted from a large number of LSC produced by an artificial training merging process and is presented detailed in optimization results. In our study, we used a Debian GNU/Linux 10.0 system (<https://www.debian.org/releases/stable/> (accessed on 10 June 2022)) and GRASS GIS 7.6.0 software to invoke the vector commands of v.category, v.edit and v.dissolve (<https://grass.osgeo.org/grass80/manuals/vector/> (accessed on 10 June 2022)) and execute the multi-scale optimization of USSUs and OSSUs.

4. Results

4.1. Global Optimal Subdivision Scale

Considering the diversity of the Yuqu River Basin, the t parameter attempted to set additional multiple values, from $50 \times 10^4 \text{ m}^2$ to $150 \times 10^4 \text{ m}^2$ with an interval of $25 \times 10^4 \text{ m}^2$. The other parameters were set as the recommended defaults [5,14,15,39] (Table 2). There were 30 valid terrain subdivisions obtained from different combinations of the (t, c) parameters. Figure 5 shows 8 of the 30 results, from the finest to the coarsest SU partitioning, from the upper left corner of $(50, 0.1)$ to the lower right corner of $(150, 0.6)$. The level of detail of the SUs' subdivisions depends heavily on the changes in parameter combinations of (t, c) , especially the parameter t . However, the parameter t was considered as having no explicit geomorphological meaning and it was suggested to have a large value ($500 \times 10^4 \text{ m}^2$) in previous studies [14,15,39]. Compared with the reference SUs, extremely large or extremely small t (such as 50 or $150 \times 10^4 \text{ m}^2$) cannot produce a proper subdivision of the landscape.

Table 2. Parameters settings for r.slopeunits.

Parameter	Value Setting
Initial flow accumulation threshold (t)	$(50, 75, 100, 125, 150) \times 10^4 \text{ m}^2$
Minimum circular variance (c)	$(0.1, 0.2, 0.3, 0.4, 0.5, 0.6)$
Minimum surface area (a)	$300,000 \text{ m}^2$
Reduction factor (r)	11
Cleaning size	$15,000 \text{ m}^2$

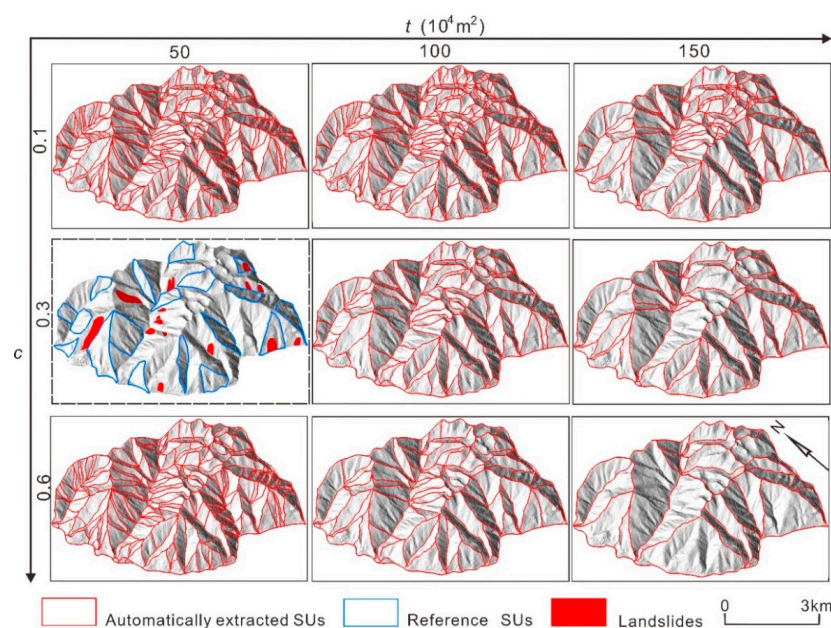


Figure 5. Examples of 9 SU terrain subdivisions for part of the Yuqu River Basin. The blue lines are reference SUs through a semi-automatic hydrological analysis method. Latitude/longitude: $28^{\circ}35'10'' \sim 28^{\circ}41'53''$, $98^{\circ}24'11'' \sim 98^{\circ}35'56''$.

The quantitative indicators of *OCE* and *GS* were thoroughly exploited to determine the optimal scale. Firstly, the errors between 952 reference SUs and the corresponding extracted SUs of different scales were calculated. As is shown in Figure 6a, the errors were at a consistently high level at the finer scale. With the gradual increase of *t* from 50 to $100 \times 10^4 \text{ m}^2$, the errors decreased accordingly until they stabilized. However, the errors increased again as *t* continuously increased to $150 \times 10^4 \text{ m}^2$. The evolution features of *OCE* are significant because they are consistent with the three stages of over-subdivision, optimal-subdivision and under-subdivision as scale increases scale. The evolution trend analysis indicates that the *t* of $100 \times 10^4 \text{ m}^2$ represents an appropriate scale.

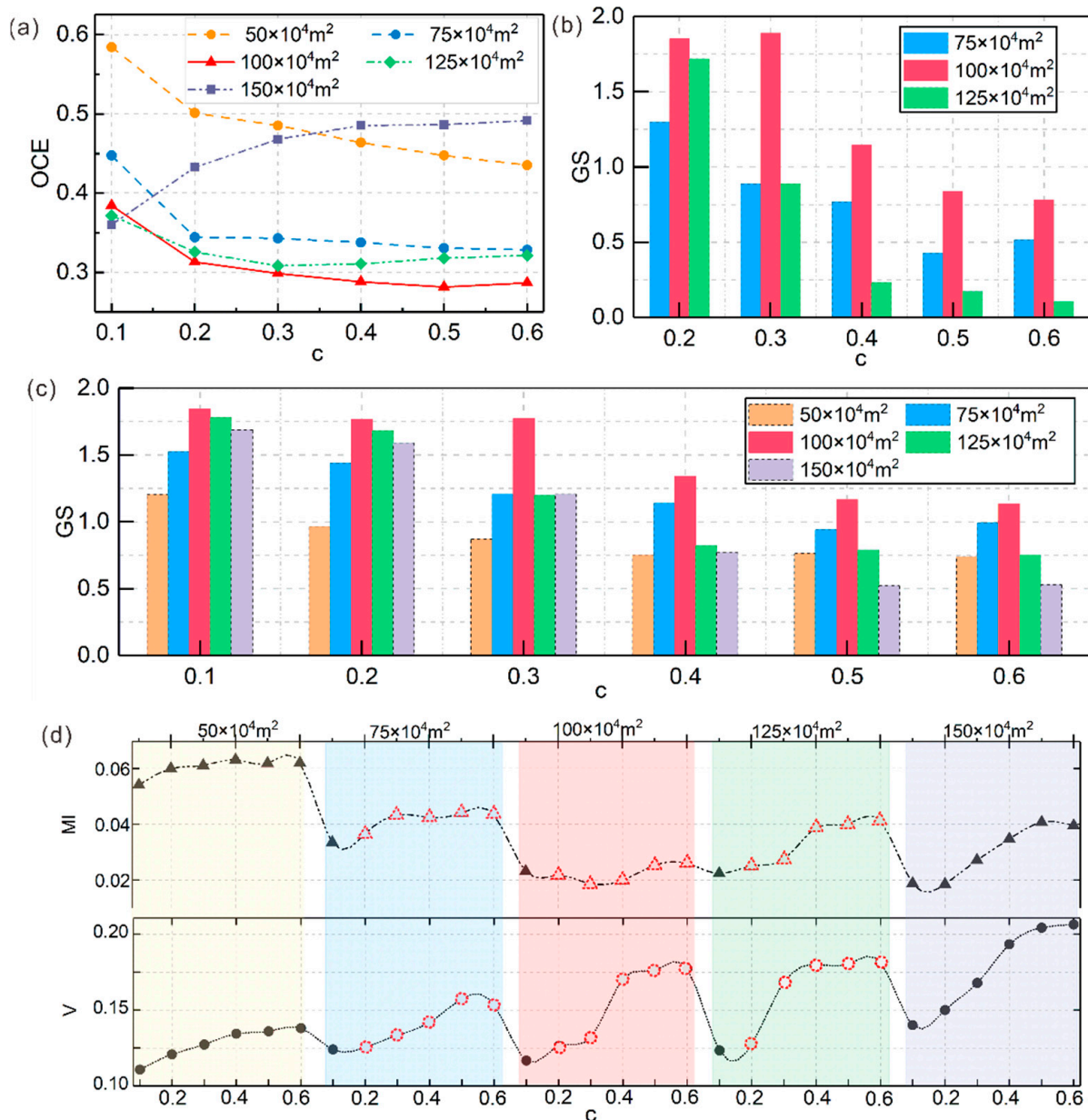


Figure 6. The global function values of SUs. (a) is the *OCE*, (b) is *GS* for the remaining 15 SUs with *OCE* under 0.35. (c,d) are the *GS* and global *MI*, global *V* of 30 SUs, respectively. The red dotted icons in (d) indicate the *MI* and *V* involved in the calculation of *GS* of (b).

Furthermore, there were 15 groups of SUs selected as meaningful subdivisions to perform the normalization step, when *OCE* < 0.35 was set as the screening criterion. They are SUs' groups with the parameter combinations of *t* (75, 100, 125) and *c* (0.2, 0.3, 0.4, 0.5,

0.6). The *GS* value of those candidate groups is shown in Figure 6b. The maximum *GS* is 1.88 with the parameter combination of (100, 0.3), indicating that both internal homogeneity and external heterogeneity are the greatest. This is selected global optimal SUs' subdivision in this paper. As a comparison, under the method of Alvioli et al. [14,15] and Jacobs et al. [5] without the inspection of the *OCE*, the *GS* was calculated in Figure 6c. The highest *GS* value of all 30 groups was 1.83 produced by the parameter combinations of (100, 0.1), which would be judged as optimal under the existing method. However, the SUs of (100, 0.1) are distinctly over-subdivided for the landscape (Figure 5) and the *OCE* is accordingly as high as 0.38. The scale of (100, 0.3) from the new proposed method is more appropriate for the selection of the optimal scale.

To understand why different optimal scales are generated by the two methods, each *MI* and *V* in the calculation of *GS* were collected in Figure 6d. The *MI* and *V* indices of different scales SUs groups varied widely. Following the gradual increase of the scale parameters, the holistic trend of *MI* index went through reduction, stabilization and increase successively, and the *V* index increased monotonically. With the candidate SUs' groups increasing from 15 to 30 or even 100, the maximum or minimum of *MI* and *V* may show new changes and eventually an uncertain optimal scale is generated. It is originated from the absence of an effective screening mechanism and an inherent drawback of unsupervised evaluation. Therefore, the candidate groups can be confirmed by retaining only meaningful subdivisions when jointing the supervised evaluation of *OCE*, thus producing a stable and consistent optimal scale. This complementary evaluation strategy is a significant improvement over the existing method.

4.2. Identification Result of USSUs and OSSUs

In this section, the OSSUs, MSSUs and USSUs were distinguished at the selected optimal scale. The frequency distribution with three kinds of *LS* are shown in Figure 7. In the No A condition (Figure 7a), the frequency of *LS* appeared to be relatively concentrated in the range of $[-1.0, 0]$, and the frequency of the cumulative curve did not show discontinuity characteristics, as expected. In Figure 7b,c, instead, the frequency followed a normal distribution, and emerged with good discontinuity at the ends. Further, compared to A and B condition, the frequency of No B condition was more concentrated in the middle interval of *LS*, and less distributed at high values, implying that more SUs may be identified as MSSUs and insufficient SUs are classified into OSSUs.

Consequently, the thresholds of discontinuity points were calculated from the frequency cumulative curve via the Otsu method [43]. The results were summarized in Table 3 and typical examples of classification were given in Figure 7d–f. For the No A condition, due to the absence of neighborhood variability, poor discriminative power was exhibited for all three types of SUs, both in terms of quantity and accuracy (Figure 7d). Subsequently, the recognition capability of USSUs was improved in No B condition, as only the SU with distinct differences from its surrounding SUs were identified as USSUs, and the proportion descended from 61.14% to 3.14% (Table 3). However, many SUs with narrow and long boundaries were still wrongly selected as MSSUs and the recognition ability for OSSUs was insufficient (Figure 7e). Once spatial weight and neighborhood variability both functioned during the identification process, more SUs was marked as OSSUs, with an increase from 8.31% to 14.6%. The USSUs are also more reasonable, with large SUs correctly distinguished and small SUs excluded (Figure 7f). The threshold ranges of USSUs, MSSUs and OSSUs are $[-1, -0.4]$, $[-0.4, 0.6]$ and $[0.6, 1]$, respectively.

Table 3. Classification threshold and corresponding proportion of MSSUs, USSUs and OSSUs.

Feature Selection	USSUs Threshold	MSSUs Threshold	OSSUs Threshold	USSUs Percentage	OSSUs Percentage
No A	(−1.0~0.60)	(−0.60~0.90)	(0.90~1.0)	61.14%	4.28%
No B	(−1.0~0.35)	(−0.35~0.60)	(0.55~1.0)	3.41%	8.31%
A and B	(−1.0~0.40)	(−0.40~0.60)	(0.60~1.0)	1.63%	14.6%

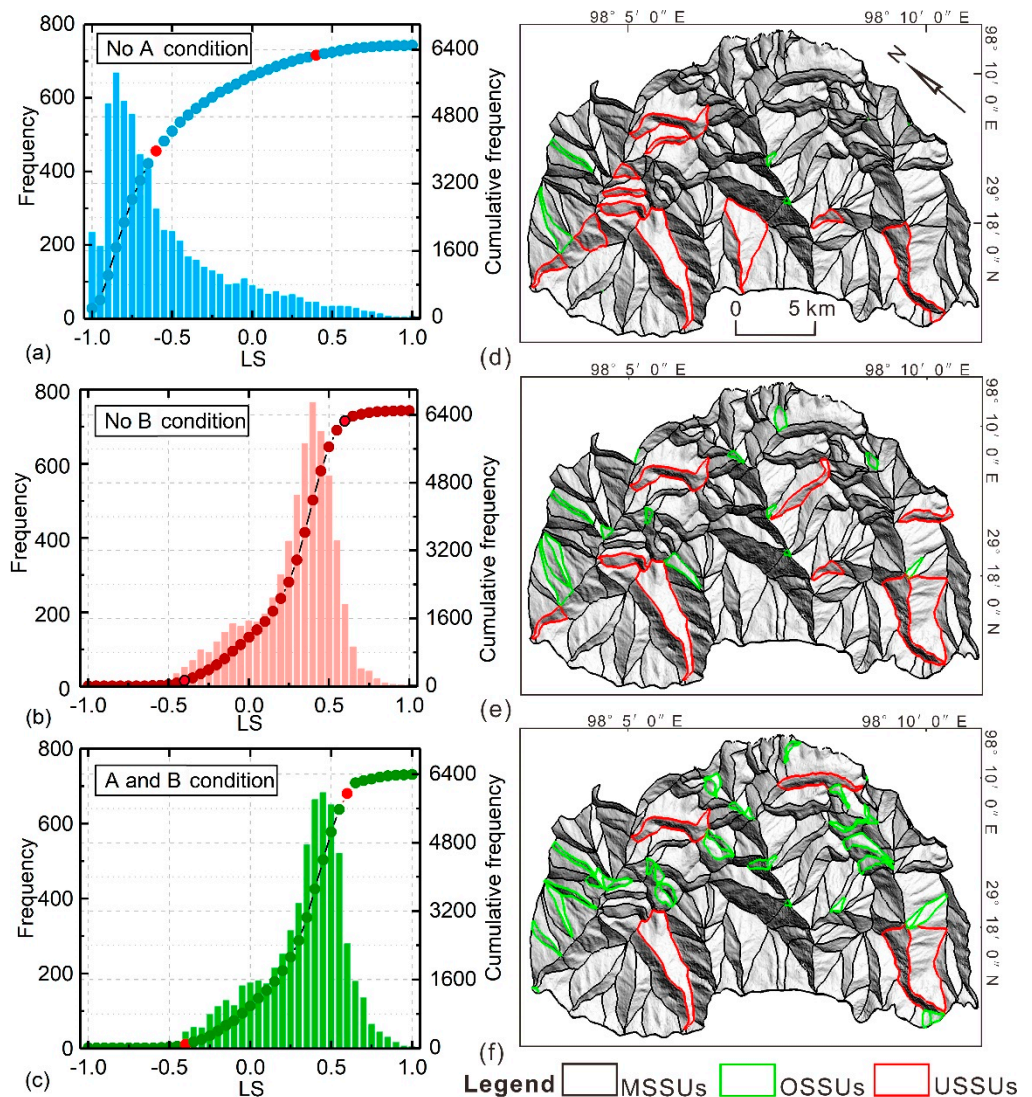


Figure 7. The classification for USSUs, OSSUs and MSSUs from three different calculation methods. (a–c) is the frequency distribution and discontinuity point respectively by No A, No B, and A and B condition. The corresponding classification results are shown in (d–f).

Figure 8 shows the spatial distribution of each type of SU in the Yuqu River Basin. A total of 6514 SUs, 106 cases of USSUs with an average area of $3.47 \times 10^6 \text{ m}^2$, and 952 cases of OSSUs with an average area of $2.41 \times 10^5 \text{ m}^2$. As details are shown in local regions, the large SUs that divided the whole gentle valley into one SU are correctly classified as USSUs (Figure 8a), and the narrow polygons formed by the interference of broken steep terrain are labeled as OSSUs (Figure 8b,c). Therefore, the method proposed for identifying USSUs and OSSUs is practicable.

4.3. Multi-Scale Optimization of Undesirable SUs

According to the multi-scale optimization method proposed in Section 3.4, ascertaining the merging threshold of the OSSUs is crucial. Some of the samples are shown in Figure 9a,b. There are 392 MSSUs obtained at the selected optimal scale (100, 0.3) and 1009 SUs assumed as OSSUs in the corresponding region at the finer scale (75, 0.3). A total of 1637 reference LSC values gained pass through five simulation merging processes (Table 4). The frequency distribution of LSC in each iteration is shown in Figure 9c; the main interval gradually increases with upper limit. Therefore, the frequency cumulative curve is constructed by

summarizing the LSC of five merges. A value below 95% of all LSC is selected as the final merging criteria, that is, $LSC_T < 0.50$.

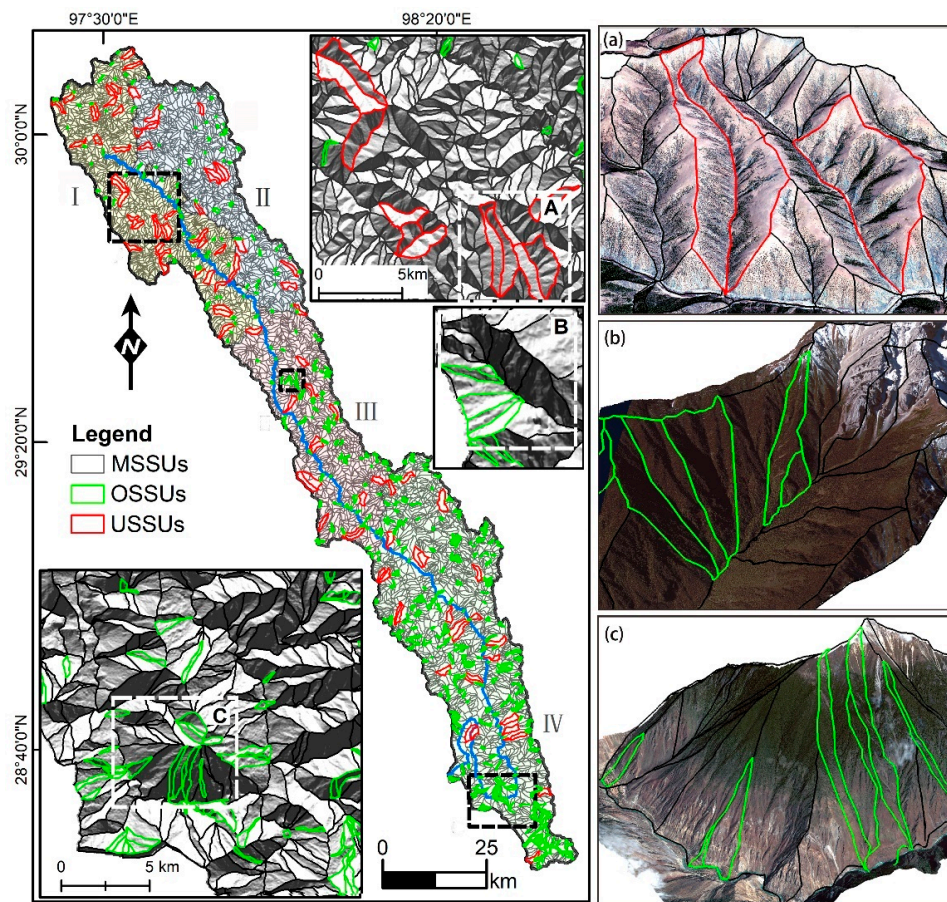


Figure 8. Left is the map of spatial distribution of MSSUs, USSUs and OSSUs in the Yuqu River Basin. Right: (a–c): the local details correspond to areas of the left A, B, C.

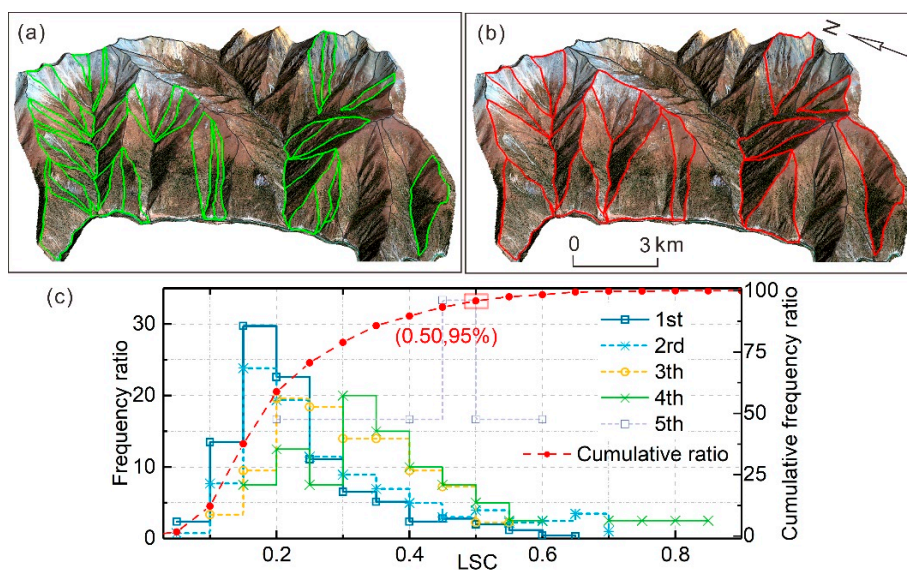


Figure 9. Process of determining the referenced threshold from the simulation merging process. (a) are examples of OSSUs from finer scale (75, 0.3), and (b) are examples of MSSUs in corresponding regions from optimal scale (100, 0.3). (c) is the frequency distribution of LSC value produced by five merging.

Table 4. Statistical table of artificial merging process from OSSUs to MSSUs.

Sequence	Total Number	New Completed	Not Done	Completed Proportion
Initial SUs		0	1009	0%
1st merging	1009	214	403	54.59%
2rd merging	617	138	179	89.79%
3th merging	531	27	40	96.68%
4th merging	419	9	6	98.97%
5th merging	398	4	0	100%
Total		392	1637	

Subsequently, the gradual optimization process is shown in Figure 10. The original SUs at the selected optimal scale of (100, 0.3) (Figure 10a) are categorized as OSSUs, MSSUs, USSUs (Figure 10b). As the second operation, the USSUs were replaced with the corresponding three finer SUs of (100, 0.2), (75, 0.2) and (75, 0.3), respectively. The substitution with the largest GS value of (100, 0.2) was considered the appropriate re-subdividing SUs. As is shown in Figure 10c, those USSUs of super-large area were effectively partitioned into two to four more refined SUs. There are 756 finer SUs generated by the re-subdividing process of the 106 USSUs and re-classified as OSSUs (Table 5). In compliance with the merging criteria of $LSC_T < 0.5$, 1708 SUs were merged for the first time and 867 SUs required a next merge iteration. Finally, the same merging iterations were executed four times until the new LSC did not meet the condition. 1058 undesirable SUs were refined into 1117 appropriate SUs with the scale combinations of (100, 0.2), (100, 0.3) and other coarser scales. The OCE was improved to as low as 0.22 with a decrease of 27%.

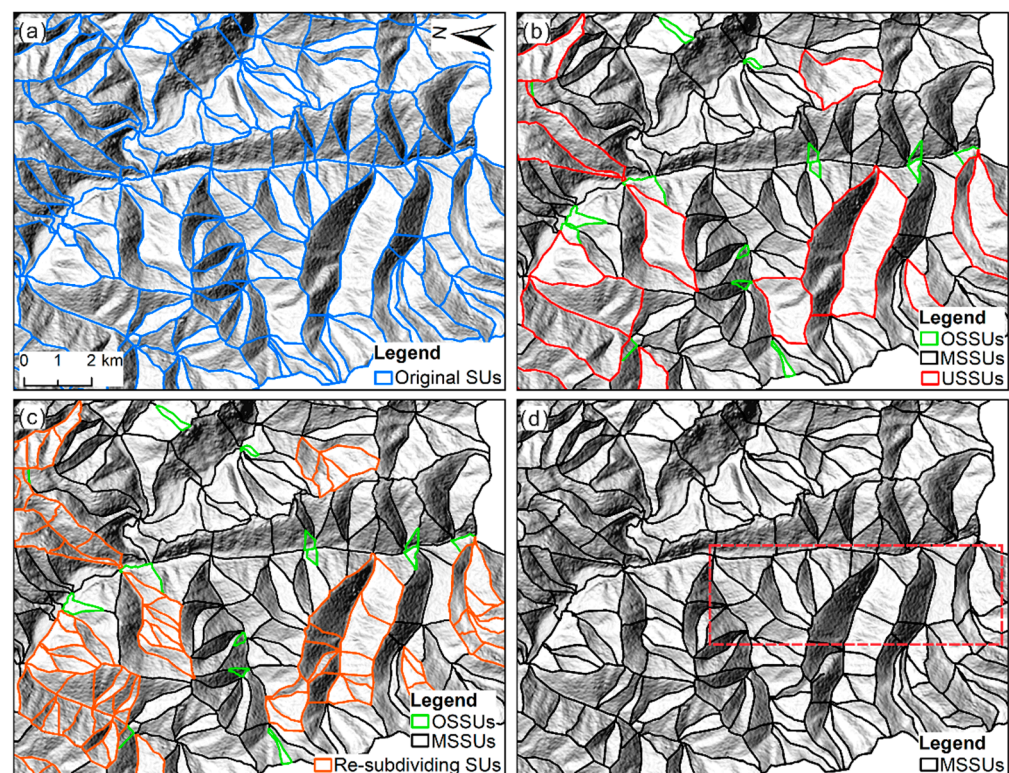


Figure 10. Gradual optimization process by the proposed method. (a) are the original SUs at optimal scale of (100, 0.3). (b) are the classification for the original SUs before refining. (c) are the first operation of replacing the USSUs with finer scale of (100, 0.2). (d) is the final MSSUs after refining unrealistic SUs.

Table 5. Statistical table of gradual optimization process from OSSUs and USSUs to MSSUs.

Classification	Initial State		Replacement	1st Merging		4th Merging			
	Number	OCE	New SUs	Number	LSC < 0.5	New SUs	LSC < 0.5	OCE	
OSSUs	952	0.30	0	1708	880	17	0	0.22	
USSUs	106		756		415				
MSSUs	5456		0		0				1100
Total	6514		756		7164				1295

With the aid of the field photography, a detailed comparison between the SUs of a single optimal scale and refined SUs after multi-scale recombination was carried out in the red box marked in Figure 10. As is shown in Figure 11c, almost each SU has achieved accurate matching with the terrain discontinuous line. Those tiny OSSUs without any terrain meaning have been merged with adjacent larger SUs. The USSUs of watersheds or large valleys have been re-subdivided along the inherent aspect turnings. Through comparing the SUs of yellow dashed lines, the refined SUs have better performance than the original SUs (Figure 11b) in terms of consistency with the actual scene. Therefore, the proposed multi-scale optimization method has well improved the limitation of matchless between the SUs and the geomorphologic background under a single scale.

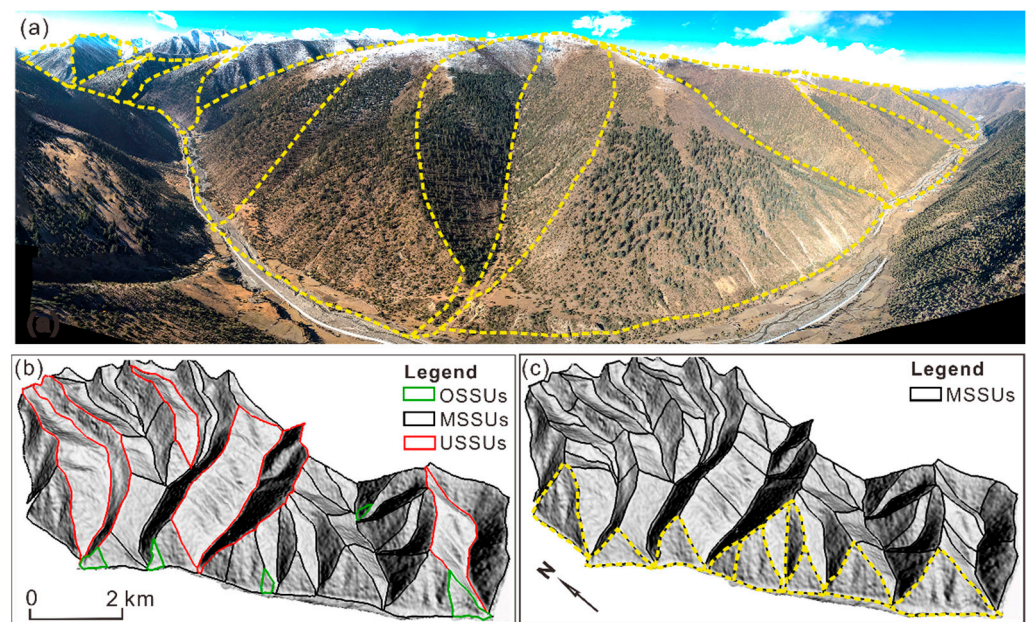


Figure 11. Comparison between the original SUs at single optimal scale and the refined SUs after multi-scale recombination. (a) is the field photo for verification, (b) are the original SUs before improvement. (c) are the final refined SUs achieved by the proposed optimization method, and the yellow dashed line marks the corresponding SUs in (a).

5. Discussion

5.1. Rationality of the Evaluation and Post-Processing for the Optimal Scale

The existing measures cannot address issues in determining the input scale parameter for the automatic delineation of SUs. Additionally, there is a lack of subsequent solution for unrealistic SUs generated from a single optimal subdivision, especially in complex terrains. This paper applied an effective subdivision quality evaluation and multi-scale refinement approach to improve consistency in a complex natural landscape. The parameters and criteria involved in the improved method are objective and can be established independently from the geographical extent. It is the first application for the improvement of individual SUs objects from automatic subdivision procedures in the Tibetan Plateau.

The advantages of unsupervised evaluation cooperated with supervised means for determining the optimal scale were significant. The method enriched the scientific justification for matching between the global optimal scale and the actual land surface discontinuities. The uncertainty in calculating the *GS* value was removed through defining qualified candidate SUs' groups. Compared to previous research [14,15,39], the *OCE* could serve as a new supervised evaluation tool for comparing terrain subdivision algorithms and adjusting the subdivision parameters. The 952 reference samples used for this study are compliant with the standard SU definition, sampling from the entire basin at equal intervals. They are capable of representing the local topography and actual land surface discontinuities. The *OCE* can be used to reliably quantify the error with the subdivision SUs with different levels of details. The discrepancy value during the process of the overgrowth parameters can be sensitively confirmed, as the *OCE* accordingly went through the decreasing, plateauing and increasing phases. Moreover, the cooperative evaluation application was sequential. The *OCE*, acting as supervised evaluation, was first performed to filter out unrealistic terrain subdivisions, and qualified SUs groups were left to participate in the calculation of *GS* values. Consequently, the very fine scale (100, 0.1) improperly determined as the optimal subdivision by the previous method was eliminated. In addition, the parameter *t* contributed the fundamental upslope area for the calculation of the orientation average value and circular variance and should be dealt with as prudently as parameter *c*.

Further, the spatial characteristics of each SU's area, boundary and aspect were sufficiently emphasized and effectively integrated during the processes of identification and optimization. The measuring of local homogeneity and heterogeneity for each SU was ingenious and practicable. In particular, the variability of aspect beyond the normal level of the surrounding regions could more appropriately indicate the differences and similarities between each SU and its adjacent SUs. Due to the scarcity of available statistical properties, the diversity of the SUs size and boundary were taken into account and acted as a neutralization coefficient. Only when the difference or similarity of aspect were in accord with the features of boundaries and regions can the specificities of local heterogeneity or homogeneity be outstanding. Thus, this linkage mechanism could reduce the probability of misclassification. Although the assumption that the discontinuity of the curve was consistent with the threshold interval of the SUs' classification lacks sufficient theoretical basis, it was an efficient and reproducible objective method. Compared with the single optimum parameter optimal, those regions with special landforms demanded other coarser or finer parameters. Both the re-subdivided with the finer scale for USSUs and the re-merged with adjacent SUs for OSSUs were defined as detailed operation guidelines. An effective examination criterion was implemented for the two refinement stages, and the reference knowledge was obtained through many manual merging training processes. After a series of identification, re-subdivision and merging processes, the SUs' groups consisting of multiple scales were achieved. This is currently one of the few available methods for non-single scales.

5.2. Terrain-Adaptive Performance of the SUs Subdivision

Owing to the complex terrains of the Yuqu River Basin and the diversity of thousands of SUs, evaluating the performance of the SUs' subdivision against the corresponding topographic feature was not an easy target. The density, spatial scale, and spatial morphology of the SUs in four topographic patterns were statistically analyzed. In general, the slopes tended to be long and large at the bigger relative relief with severe geomorphic cutting, so the density, size and shapes of SUs should be distinguished from those of small and low elevation differences. Firstly, the I, II, III and IV geomorphic regions were divided into 2~4 intervals according to the 300 m interval of elevation difference. As shown in Figure 12a,b, the average density of SUs (the ratio of the number of SU to the area of the statistical interval) decreases linearly with the increase of the elevations' relative relief, and the average area of SUs increases. In the high hilly zone (I), the height difference was between 0.5~1.1 km, the SUs presented the most intensive distribution with average

density values ($1.47 \text{ SU}/\text{km}^2$), which corresponded to a large number of homogeneous low-lying hills and valleys. In the alpine gorge zone (IV), the height difference was between $1.4\sim 2.3 \text{ km}$, the average area of SUs was shown as a maximum value of 0.99 km^2 , which is in accordance with a tall valley formed by the rapid river downcutting.

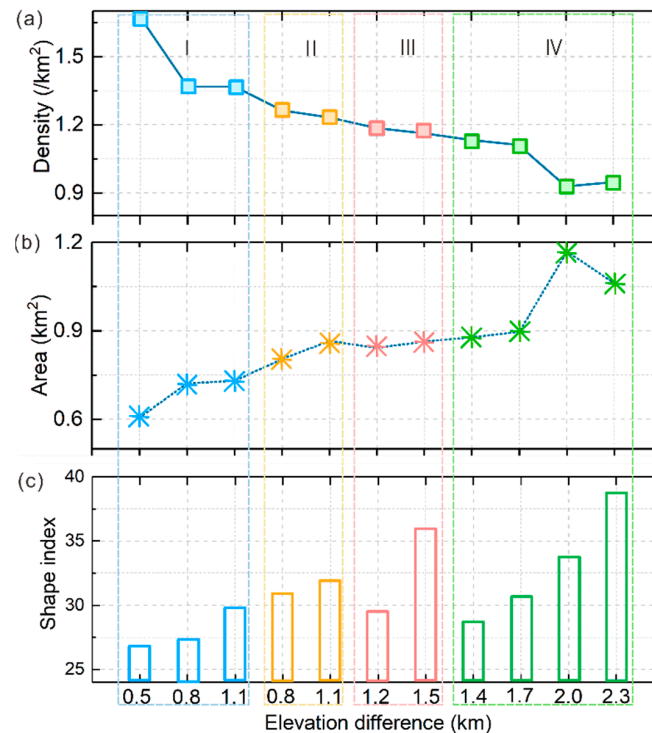


Figure 12. Statistical result of spatial distribution characteristics for the SUs. (a–c) is the average density, average area and shape index of the SUs in in I, II, III and IV topographic patterns, respectively.

In addition, the shapes of SUs were also sensitive to various topographic features. The shape index (R index) was calculated using the equation from Hang et al. [18,45], which was the ratio of the square of the perimeter to the corresponding area. For more narrow-flat or more strip-shaped polygons, the R index increased, such as the triangle is 20.78 and the rectangle that the length to width of 6:1 is 32.67. As shown in Figure 12c, the shape index of SUs from each geomorphic region were distinguishable. The average minimum value of the R index in the high hilly zone (I) was about 27.72, showing that the geometric shape more resembled a triangle. Even in the same height interval of $0.8\sim 1.1 \text{ km}$, the R index of the middle-high mountain zone (II) was as high as 31.5, indicating that the shape of SUs were narrower and longer. It conformed to the characteristics of mountain landscape shaped by glacier erosion. The sensitive change of the R index also existed in the interior of geomorphic regions, especially the gorge transition zone (III). The R index in the interval $[0.9\sim 1.2 \text{ km}]$ connecting the broad and gentle landform in the upper reach was 27.01, implying a more uniform shape of aspect ratio of the SUs. However, the R index was 34.05, up 25% in the interval of $[1.2\sim 1.5 \text{ km}]$ transition to deep canyon landform, corresponding to a narrow strip shape change of SUs. Therefore, the multi-scale optimization of SUs was able to capture the morphological variability of the landscape and divided the study area into SUs with different shapes and sizes.

6. Conclusions

A set of appropriate SUs that properly partition a complex landscape into reasonable terrain subdivisions is crucial for landslide sensitivity modeling. Difficulties in determining the input scale parameters and the absence of subsequent amending procedures have restrained the wide application of existing automatic extraction methods. An improved au-

automatic subdivision quality evaluation and multi-scale refinement method were proposed in this paper. An evaluation approach coordinated with supervised and unsupervised means were exploited. The *OCE* value is an effective discrepancy metric that can inhibit the uncertainty existing in optimal scale from the combination of global variance and global *MI*. Multiple space geometry features and aspects were effectively integrated into the process of the identification and refinements of undesirable SUs. In the example region, 6514 SUs were automatically obtained at the optimal subdivision scale, of which 106 cases were distinguished as USSUs and 956 were OSSUs. To better deal with unreasonable SUs at the selected single optimal scale, an effective optimization mechanism was established. The final SUs' groups composed of terrain subdivisions with multiple scales were achieved, which is an infrequently available method for non-single scales. Field investigations and statistical distribution characteristics have demonstrated the excellent performance of the SUs for the corresponding geomorphological reality. With improved organization and distribution of geoenvironmental data, the refining SUs have great application potential in landslide sensitivity modeling and other situations that require the identification of homogeneous terrain domains.

Supplementary Materials: The following supporting information can be downloaded at: <https://www.mdpi.com/article/10.3390/rs14143444/s1>, the information of original data used in Figures 6, 7 and 9, Table S1 Supplementary Material of Figures 6, 7 and 9.

Author Contributions: Z.Y.: Software, Investigation, Writing—Original Draft; J.W.: Conceptualization, Validation, Writing—Review and Editing, Funding acquisition; J.D.: Resources, Conceptualization, Project administration; S.Z.: Investigation, Methodology and Validation. All authors have read and agreed to the published version of the manuscript.

Funding: This study was financially supported by National Natural Science Foundation of China (No. 41977246) and National Key R&D Program of China (2018YFC1505006).

Data Availability Statement: The GNU/Linux system was obtained from (<https://www.debian.org/releases/stable/>, accessed on 10 April 2022) and GRASS GIS 7.8.1 was provided by project of the Open Source Geospatial Foundation (OSGeo) (<https://grass.osgeo.org/download/windows/>, accessed on 10 April 2022). The Software of r.slopeunits v1.0 was obtained from the Portal of the Geomorphology Research Group (<http://geomorphology.irpi.cnr.it/tools/slope-units>, accessed on 10 April 2022). The Gaofen-2 satellite data and ALOS-12m DEM data are provided by a third party, not a public dataset. The source data used in the analysis of this paper have been uploaded on as Supplementary Table S1.

Conflicts of Interest: The authors declare no conflict of interest.

Abbreviations

Variable	Description	First Introduced
<i>a</i>	Minimum surface area (m ²)	r.slopeunits parameter
<i>c</i>	Minimum circular variance	r.slopeunits parameter
<i>t</i>	the initial flow accumulation area threshold (m ²)	r.slopeunits parameter
<i>r</i>	Reduction factor	r.slopeunits parameter
<i>OCE</i>	the object-level consistency error	Equation (1)
<i>MI</i>	Moran's I index	Equation (3)
<i>V</i>	Variance index	Equation (4)
<i>GS</i>	the global heterogeneity score	Equation (5)
<i>D^a</i>	the neighborhood variability of aspect difference	Equation (6)
<i>D^{sd}</i>	the neighborhood variability of the standard deviation	Equation (8)
<i>r^a</i>	the area ratio of SU to its total area of adjacent units	Equation (9)
<i>r^l</i>	the degree of coincidence of the common boundary	Equation (10)
<i>he^L</i>	Local heterogeneity	Equation (11)
<i>ho^L</i>	Local homogeneity	Equation (12)
<i>LS</i>	the average local similarity	Equation (13)
<i>LSC</i>	the average local similarity change	Equation (14)

References

1. Guzzetti, F.; Reichenbach, P.; Ardizzone, F.; Cardinali, M.; Galli, M. Estimating the quality of landslide susceptibility models. *Geomorphology* **2006**, *81*, 166–184. [[CrossRef](#)]
2. Reichenbach, P.; Rossi, M.; Malamud, B.; Mihir, M.; Guzzetti, F. A review of statistically-based landslide susceptibility models. *Earth-Sci. Rev.* **2018**, *180*, 60–91. [[CrossRef](#)]
3. Evans, I. Geomorphometry and landform mapping: What is a landform? *Geomorphology* **2012**, *137*, 94–106. [[CrossRef](#)]
4. Xie, M.; Esaki, T.; Zhou, G. GIS-Based Probabilistic Mapping of Landslide Hazard Using a Three-Dimensional Deterministic Model. *Nat. Hazards* **2006**, *33*, 265–282. [[CrossRef](#)]
5. Jacobs, L.; Kervyn, M.; Reichenbach, P.; Rossi, M.; Marchesini, I.; Alvioli, M.; Dewitte, O. Regional susceptibility assessments with heterogeneous landslide information: Slope unit- vs. pixel-based approach. *Geomorphology* **2020**, *356*, 107084. [[CrossRef](#)]
6. Malamud, B.; Reichenbach, P.; Rossi, M.; Mihir, M. Report on Standards for Landslide Susceptibility Modelling and Terrain Zonations, LAMPRE FP7 Project Deliverables. 2014. Available online: <http://www.lampre-project.eu> (accessed on 3 November 2014).
7. Minár, J.; Evans, I. Elementary forms for land surface segmentation: The theoretical basis of terrain analysis and geomorphological mapping. *Geomorphology* **2008**, *95*, 236–259. [[CrossRef](#)]
8. Carrara, A.; Cardinali, M.; Detti, R.; Guzzetti, F.; Pasqui, V.; Reichenbach, P. GIS techniques and statistical models in evaluating landslide hazard. *Earth Surf. Process. Landf.* **1991**, *16*, 427–445. [[CrossRef](#)]
9. Guzzetti, F.; Carrara, A.; Cardinali, M.; Reichenbach, P. Landslide hazard evaluation: A review of current techniques and their application in a multi-scale study, Central Italy. *Geomorphology* **1999**, *31*, 181–216. [[CrossRef](#)]
10. Turel, M.; Frost, J. Delineation of Slope Profiles from Digital Elevation Models for Landslide Hazard Analysis. In Proceedings of the GeoRisk 2011: Geotechnical Risk Assessment and Management, Atlanta, GA, USA, 26–28 June 2011; American Society of Civil Engineers: Reston, VA, USA, 2011; pp. 829–836.
11. Bornaetxea, T.; Rossi, M.; Marchesini, I.; Alvioli, M. Effective surveyed area and its role in statistical landslide susceptibility assessments. *Nat. Hazards Earth Syst. Sci.* **2018**, *18*, 2455–2469. [[CrossRef](#)]
12. Xie, M.; Esaki, T.; Qiu, C.; Wang, C. Geographical information system-based computational implementation and application of spatial three-dimensional slope stability analysis. *Comput. Geotech.* **2006**, *33*, 260–274. [[CrossRef](#)]
13. Romstad, B.; Etzelmuller, B. Mean-curvature watersheds: A simple method for segmentation of a digital elevation model into terrain units. *Geomorphology* **2012**, *139*, 293–302. [[CrossRef](#)]
14. Alvioli, M.; Marchesini, I.; Reichenbach, P.; Rossi, M.; Ardizzone, F.; Fiorucci, F.; Guzzetti, F. Automatic delineation of geomorphological slope units with r.slopeunits v1.0 and their optimization for landslide susceptibility modeling. *Geosci. Model Dev.* **2016**, *9*, 3975–3991. [[CrossRef](#)]
15. Alvioli, M.; Guzzetti, F.; Marchesini, I. Parameter-free delineation of slope units and terrain subdivision of Italy. *Geomorphology* **2020**, *358*, 107124. [[CrossRef](#)]
16. Wang, K.; Zhang, S.; DelgadoTéllez, R.; Wei, F. A new slope unit extraction method for regional landslide analysis based on morphological image analysis. *Bull. Eng. Geol. Environ.* **2018**, *78*, 4139–4151. [[CrossRef](#)]
17. Zhang, T.; Fu, Q.; Quevedo, R.; Chen, T.; Luo, D.; Liu, F.; Kong, H. Landslide Susceptibility Mapping Using Novel Hybrid Model Based on Different Mapping Units. *KSCE J. Civ. Eng.* **2022**, *26*, 2888–2900. [[CrossRef](#)]
18. Huang, F.; Tao, S.; Chang, Z.; Huang, J.; Fan, X.; Jiang, S.; Li, W. Efficient and automatic extraction of slope units based on multi-scale segmentation method for landslide assessments. *Landslides* **2021**, *18*, 3715–3731. [[CrossRef](#)]
19. Li, Y.; He, J.; Chen, F.; Han, Z.; Wang, W.; Chen, G.; Huang, J. Generation of Homogeneous Slope Units Using a Novel Object-Oriented Multi-Resolution Segmentation Method. *Water* **2021**, *13*, 3422. [[CrossRef](#)]
20. Mergili, M.; Marchesini, I.; Alvioli, M.; Metz, M.; Schneider-Muntau, B.; Rossi, M.; Guzzetti, F. A strategy for GIS-based 3-D slope stability modelling over large areas. *Geosci. Model Dev.* **2014**, *7*, 2969–2982. [[CrossRef](#)]
21. Dekavalla, M.; Argyalás, D. Evaluation of a spatially adaptive approach for land surface classification from digital elevation models. *Int. J. Geogr. Inf. Sci.* **2017**, *31*, 1978–2000. [[CrossRef](#)]
22. Zhao, M.; Li, F.; Tang, G. Optimal Scale Selection for DEM Based Slope Segmentation in the Loess Plateau. *Int. J. Geosci.* **2012**, *3*, 37–43. [[CrossRef](#)]
23. Hu, Z.; Zhang, Q.; Zou, Q.; Li, Q.; Wu, G. Stepwise Evolution Analysis of the Region-Merging Segmentation for Scale Parameterization. *IEEE J. Sel. Top. Appl. Earth Obs. Remote Sens.* **2018**, *11*, 2461–2472. [[CrossRef](#)]
24. Espindola, G.; Camara, G.; Reis, I.; Bins, L.; Monteiro, A. Parameter selection for region-growing image segmentation algorithms using spatial autocorrelation. *Int. J. Remote Sens.* **2006**, *27*, 3035–3040. [[CrossRef](#)]
25. Polak, M.; Zhang, H.; Pi, M. An evaluation metric for image segmentation of multiple objects. *Image Vis. Comput.* **2009**, *27*, 1223–1227. [[CrossRef](#)]
26. Hu, Z.; Li, Q.; Zhang, Q.; Zou, Q.; Wu, Z. Unsupervised Simplification of Image Hierarchies via Evolution Analysis in Scale-Sets Framework. *IEEE Trans. Image Process.* **2017**, *26*, 2394–2407. [[CrossRef](#)]
27. Chen, J.; Deng, M.; Mei, X.; Chen, T.; Shao, Q.; Hong, L. Optimal segmentation of a high-resolution remote-sensing image guided by area and boundary. *Int. J. Remote Sens.* **2014**, *35*, 6914–6939. [[CrossRef](#)]
28. Louw, G.; van Niekerk, A. Object-based land surface segmentation scale optimisation: An ill-structured problem. *Geomorphology* **2019**, *327*, 377–384. [[CrossRef](#)]

29. Shi, X.; Li, Y.; Zhao, Q. Flexible Hierarchical Gaussian Mixture Model for High-Resolution Remote Sensing Image Segmentation. *Remote Sens.* **2020**, *12*, 1219. [[CrossRef](#)]
30. Cheng, Y.; Mao, F. Selection of the Optimal Segmentation Scale in High-resolution Remote Sensing Image. *DEStech Trans. Comput. Sci. Eng.* **2018**, *26*, 1175–1184. [[CrossRef](#)]
31. Dadgar, A.; Baleghi, Y.; Ezoji, M. Improved Object Matching in Multi-Objects Tracking Based on Zernike Moments and Combination of Multiple Similarity Metrics. *Int. J. Eng.* **2021**, *34*, 1445–1454. [[CrossRef](#)]
32. Chen, F.; Liao, G. *The Basic Geological Characteristics in Qamdo District. Contribution to the Geology of the Qinghai-Xizang (Tibet) Plateau, 1983*; Geological Publishing House: Beijing, China, 1984; pp. 213–228.
33. Zhang, W.; Tang, Q.; Liu, L.; Shen, J.; Li, Y.; Cheng, R. Geomorphologic analysis of Yuqu River Drainage basin in Tenasserim Chain Based on Hypsometric Integral Value. *Sci. Geogr. Sin.* **2020**, *40*, 1394–1402. [[CrossRef](#)]
34. Zhao, Z.; Liu, Z.; Xu, C. Slope Unit-Based Landslide Susceptibility Mapping Using Certainty Factor, Support Vector Machine, Random Forest, CF-SVM and CF-RF Models. *Front. Earth Sci.* **2021**, *9*, 589630. [[CrossRef](#)]
35. Wang, F.; Xu, P.; Wang, C.; Wang, N.; Jiang, N. Application of a GIS-Based Slope Unit Method for Landslide Susceptibility Mapping along the Longzi River, Southeastern Tibetan Plateau, China. *ISPRS Int. J. Geo-Inf.* **2017**, *6*, 172. [[CrossRef](#)]
36. Sun, X.; Chen, J.; Han, X.; Bao, Y.; Zhu, X.; Peng, W. Landslide susceptibility mapping along the upper Jinsha River, south-western China: A comparison of hydrological and curvature watershed methods for slope unit classification. *Bull. Eng. Geol. Environ.* **2020**, *79*, 4657–4670. [[CrossRef](#)]
37. Bellach, J.D.; Wayne, M. *Biostatistics: A foundation for analysis in the health sciences*, 4. ed. J. Wiley & Sons, New York–Chichester–Brisbane–Toronto–Singapore 1987, XIII, 734 S. S., \$33.90. *Biom. J.* **2007**, *30*, 552. [[CrossRef](#)]
38. Meng, T.; Xu, X.; Liu, H. Landslide risk assessment in high altitude areas based on slope unit optimization: Taking the Baige landslide in Jinsha River as an example. *J. Henan Polytech. Univ. Nat. Sci.* **2021**, *40*, 65–72. [[CrossRef](#)]
39. Schlögel, R.; Marchesini, I.; Alvioli, M.; Reichenbach, P.; Rossi, M.; Malet, J. Optimizing landslide susceptibility zonation: Effects of DEM spatial resolution and slope unit delineation on logistic regression models. *Geomorphology* **2018**, *301*, 10–20. [[CrossRef](#)]
40. Cai, Y.; Li, X.; Zhang, M.; Lin, H. Mapping wetland using the object-based stacked generalization method based on multi-temporal optical and SAR data. *Int. J. Appl. Earth Obs. Geoinf.* **2020**, *92*, 102164. [[CrossRef](#)]
41. Yang, Z.; Wei, J.; Deng, J.; Gao, Y.; Zhao, S.; He, Z. Mapping Outburst Floods Using a Collaborative Learning Method Based on Temporally Dense Optical and SAR Data: A Case Study with the Baige Landslide Dam on the Jinsha River, Tibet. *Remote Sens.* **2021**, *13*, 2205. [[CrossRef](#)]
42. Johnson, B.; Xie, Z. Unsupervised image segmentation evaluation and refinement using a multi-scale approach. *ISPRS J. Photogramm. Remote Sens.* **2011**, *66*, 473–483. [[CrossRef](#)]
43. Otsu, N. A Threshold Selection Method from Gray-Level Histograms. *IEEE Trans. Syst. Man Cybern.* **1979**, *9*, 62–66. [[CrossRef](#)]
44. Filali, I.; Allili, M.; Benblidia, N. Multi-scale salient object detection using graph ranking and global–local saliency refinement. *Signal Processing Image Commun.* **2016**, *47*, 380–401. [[CrossRef](#)]
45. Zhao, S.; He, Z.; Deng, J.; Li, H.; Dai, F.; Gao, Y.; Chen, F. Giant river-blocking landslide dams with multiple failure sources in the Nu River and the impact on transient landscape evolution in southeastern Tibet. *Geomorphology* **2022**, *413*, 108357. [[CrossRef](#)]